



Fabrication of a stepped optical fiber tip for miniaturized scanners

Mandeep Kaur^{a,b,c}, Geoffrey Hohert^c, Pierre M. Lane^{b,c}, Carlo Menon^{a,b,*}

^a MENRVA Research Group, Schools of Mechatronic Systems Engineering and Engineering Science, Simon Fraser University, Surrey, B.C., Canada

^b School of Engineering Science, Simon Fraser University, Burnaby, B.C., Canada

^c Imaging Unit, Integrative Oncology, BC Cancer Research Center, Vancouver, B.C., Canada

ARTICLE INFO

Keywords:

Optical fiber
Wet etching
Heating and pulling
Micrometer fiber tip
Resonant scanner

ABSTRACT

Advancements in fabrication of miniaturized optical scanners would benefit from micrometer sized optical fiber tips. The change in the cross section of an optical fiber tip is often accompanied with the presence of a longer tapered area. The reduction of the cross section of double clad optical fibers (DCF) with a flat interface surface at the region where a change in the cross section takes place (with an abrupt change in the cross section) is considered in this paper. Various methods such as heating and pulling, wet etching using hydrofluoric acid (HF), and etching in a vaporous state were explored. The optical etching rate and its dependence on the temperature of the etchant solution were also determined. Optical fibers etch linearly with time, and the etching speed is dependent on the temperature of the etchant solution which shows a parabolic trend. The flatness of the surface at the cross section change is an interesting parameter in the fabrication of submillimeter sized scanners where the light is transmitted through the core of the DCF, and reflected light is collected through the inner cladding of the same fiber, or vice versa. The surface flatness at the interface was compared among different fiber samples developed using the aforementioned techniques. This research illustrates that the wet chemical etching performed by blocking the capillary rising of etchant solution along the fiber provided advantages over the heating and pulling technique in terms of light intensity transmitted to the target sample and the reflected light collected through the interface of etched cladding.

1. Introduction

Optical fibers are cylindrical-shaped dielectric waveguides, with a central cylindrical core surrounded by an outer cylinder that has a slightly lower index of refraction. The light is transmitted through the fiber's core due to total internal reflection. Optical fiber-based devices are continuously emerging in a wide range of applications due to their capability to work in harsh environments, immunity to electromagnetic fields, feasibility to remotely monitor a process/work, and use in fabricating light-weight and compact sized devices. The applications of optical fibers include: networking systems [1]; sensing applications such as measuring air humidity [2], temperature, pressure, strain, displacement; sensing load and vibrations in an industrial plant [3]; design of traffic monitoring devices [4], and biomedical sensors. In the biomedical field, optical fibers represent a key element for endoscopic imaging used for cardiovascular imaging, angioscopy, ophthalmology, oncology, gastroenterology, neurology, dermatology, and dentistry applications [5]. There are large number of optical fiber based biomedical sensors

developed for in-vivo measurements of physical parameters such as body and tissue temperature. These biomedical sensors are mainly useful in magnetic resonance imaging (MRI) and radiofrequency (RF) hyperthermia therapy for cancer treatment, testing of pacemakers and implantable devices [6,7], pressure measurements (cardiovascular, intracranial, urological/rectal) [6,8], blood flow rate to monitor changes in microcirculation [6,9], detecting breathing conditions by monitoring the humidity in respiration [6], measuring biting force in dentistry [6], and detecting radiation dose in radiotherapy [6]. There are some other biomedical sensors developed for investigating chemical properties of body fluids to detect different diseases. Some of these fiber-optic catheter sensors are developed for detection of bile component in reflux disease (Bilitec 2000) [10], pH level in blood, tissue or gastric fluid [6], oxygen content in blood or respiration [6], carbon dioxide, etc. [11]. The recent advances in these technologies enabled the integration of optical fibers in textiles developed as wearable sensors to measure the aforementioned biological signals like heart rate and breathing, oxygen saturation, temperature etc. [12–15].

* Corresponding author at: MENRVA Research Group, Schools of Mechatronic Systems Engineering and Engineering Science, Simon Fraser University, Surrey, B.C., Canada.

E-mail address: cmemon@sfu.ca (C. Menon).

<https://doi.org/10.1016/j.yofte.2020.102436>

Received 17 September 2020; Received in revised form 29 November 2020; Accepted 8 December 2020

Available online 30 December 2020

1068-5200/© 2020 The Author(s). Published by Elsevier Inc. This is an open access article under the CC BY license (<http://creativecommons.org/licenses/by/4.0/>).

The introduction of optical fibers as light waveguides enables the miniaturization of a wide range of devices [16–18]. In the biomedical imaging field, it permits the fabrication of miniaturized endoscopic probes that can detect lesion/tumor tissue at early stages with micrometer sized resolution and assist as a guide for biopsy tools during diagnostic procedures. Various small sized optical scanning probes have been recently developed by vibrating the distal tip of a single mode optical fiber at resonance using an actuator placed few millimeters away from the free end [19–25]. The vibrating fiber shines light on the target sample, and the reflected light signal is captured by a charged-couple device (CCD)/complementary metal oxide semiconductor (CMOS) camera using an optical lens system [25], or external optical fibers placed at the periphery of the central vibrating fiber [19,26]. Analogous to the latter method, it is possible to miniaturize an optical scanning device by using a double clad fiber (DCF) where the central core of the fiber is used to shine the light on the target sample and the backscattered reflected light is collected through the inner cladding of the fiber, which is then used to reconstruct the image of the scanned object [27,28]. The scan area is dictated by the tip displacement of the distal end of the fiber, and the natural frequency of a cantilevered fiber can be increased by reducing the diameter of the vibrating portion to make it compatible with the driving frequency offered by micro-actuators [29]. The length of an etched surface or tip has an inverse relation with the natural frequency. An etched tip having a length of 2 mm is considered in this paper such that for an etched diameter of $\sim 12 \mu\text{m}$, it allows a resonant frequency of 2–3 kHz.

In other words, the performance of small sized optical scanners can be improved by extending only the core section as a cantilever. However, the fabrication of a small sized cantilever requires that the distal end of the inner cladding surface be perpendicular to the illumination path to capture the maximum amount of the incoming light. The presence of two light transporting mediums with different refractive indices in an DCF enable the characterization of the interface surface by transmitting the light through one medium and collecting the reflected light through the other medium. In the case of the application described above, it is possible to obtain fluorescence imaging where an infrared or visible light is transmitted through the core shines on the target, and the reflected fluorescent signal with the longer wavelength is collected through the inner cladding acting as a multimode light guide. The fabrication of such a stepped fiber is presented in this paper.

Optical fibers are often tapered down to get micrometer or nanometer sized fiber tips, enhancing the sensitivity of the sensor in some applications and allowing its use in scanning near-field microscopy, or in biomedical fields to monitor tissue surfaces at the cellular level [30,31]. Typically, the tapering of an optical fiber consists of smoothly reducing the diameter of the fiber. Submicron sized glass structures can be fabricated using various methods, including sandblasting [32], chemical etching [16,33–35], heating and pulling [36], focused ion beam etching [37], dry reactive ion etching [38], and laser micromachining [39]. Among these methods, chemical etching and heating and pulling are the most cost effective and feasible solutions for fiber section reduction.

In the heating and pulling method, a large amount of heat, generated by a flame, electric arc, or a high-power laser, is applied to the fiber to locally increase the temperature until it reaches its glass transition temperature. At the same time, the fiber is pulled axially to reduce the section. The tapered fiber generated with this method conserves its geometrical aspect, as the core and cladding are both reduced in dimension at the same rate [36].

Another available technique to reduce the cross section of an optical fiber is chemical etching, which predominantly uses hydrofluoric acid (HF) as an etchant. This technique is normally used to etch optical fibers to obtain nanometer sized fiber tips for use in optical sensors [33–35]. It is possible to reduce the section of optical fibers using the etchant solution in a liquid or vaporous state.

The tapered fibers with a stepped interface surface fabricated using these methods are characterized by transmitting light through the core

of the DCF towards a mirror and collecting the reflected light through the inner cladding of the fiber. A double clad fiber coupler (DCFC) is used to separate the light transmitted through the core of the fiber and the reflected signal passing through the cladding.

Both the heating and pulling, and chemical etching techniques lead to the formation of a longer tapered region at the interface surface where the reduction in diameter takes place. In this study, both of these methods were used to reduce the diameter of a glass DCF (SM-9/105/125-20A, Nufem) tip resulting in an abrupt change in the cross section (stepped fiber tip).

An optical fiber having a few millimeters long tip with a very small diameter may even find use in a variety of other optical devices and scanners such as temperature sensors [40], humidity sensors [41], or interferometers [42] depending on the type of the fiber used.

This paper is organized as follows. The fabrication process of the stepped fiber tip using heating and pulling, and the wet chemical etching method is presented in Section 2. The simulation work of the chemical etching process is reported in Section 3. The testing of the surface flatness at the stepped interface is described in Section 4. The results of the experimental work are discussed in Section 5. The conclusions for our work are provided in Section 6.

2. Experimental work

2.1. Fabrication of a cantilevered section using the heating and pulling method

In the heating and pulling method, the reduction in the cross section of an optical fiber is performed by heating the fiber and pulling it apart at the same time. The schematic diagram showing an overall fabrication process for the cantilevered tip of the fiber is illustrated in Fig. 1. First, the plastic protective jackets on the fibers were stripped away. A 125 μm Multi-Mode Fiber (MMF) with 105 μm core (MM-S105/125-22A, Nufem) was tapered down to a 12 μm outer diameter to obtain a core diameter of about 10 μm (assuming the ratio between the outer diameter and the core diameter remains same after tapering process), which closely matches the core size of a DCF fiber (outer diameter of 125 μm , and core of 9 μm). The schematic of this step is shown in Fig. 1a. Fiber tapering was achieved by heating the fiber to its glass transition temperature ($\sim 2000^\circ\text{C}$), then pulling one end at a velocity of $\sim 1.00 \text{ mm/s}$, performed automatically by a Vytran glass processing station (GPX-3000, ThorLabs). The filament power (36.0 W), delay (2.00 s), and pulling velocity (1.00 mm/s) provided a precise tension profile, generating the desired diameter for the tapered section.

The tapered fiber was then cleaved off with a precision diamond blade scribe providing a quasi-flat and perpendicular glass end face, as

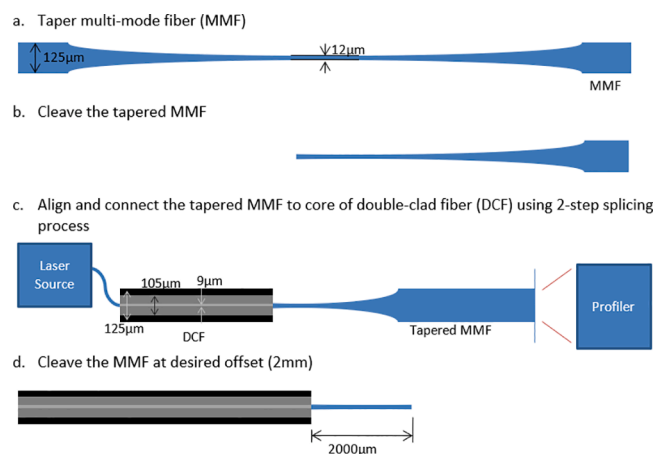


Fig. 1. Schematic of fabrication process of the cantilever fiber using the heating and pulling method.

in Fig. 1b. The tapered fiber was then aligned with the DCF core by connecting the proximal end of the DCF to a laser and monitoring the maximum relative power transmitted through the aligned fiber cores, as schematized in Fig. 1c. Usually, the maximum transmitted light varied from 60% to 90% of the incoming light, depending on fabrication imperfections. The fibers were then spliced using a two-step splicing method aligning their cores. In the first step, the fiber tips were slightly melted and connected with a hot push of 8.0 μm and 47.0 W of filament power for 2.00 s. Secondly, more power was applied to strengthen the connection optically and mechanically by applying a filament power of 50.0 W with no hot push. The spliced MMF was then cleaved off at the desired length (2.00 mm in our case) from the spliced region (Fig. 1d). The two-step splicing process allowed a firm connection minimizing distortion at the splice joint.

2.2. Fabrication of a cantilevered section using the chemical etching method

In the chemical etching method, the fiber was submerged in an etchant solution until it reaches the desired dimensions. The geometrical aspect of the fiber was changed by dissolving only the outer cladding surface. The reaction between HF and the fiber surface is characterized by one of the following reactions (1) or (2).



The first reaction is dominant in diluted HF solutions, while the second one prevails in concentrated etchant solutions [43]. The surface etching reactions described above are a simplification of the actual reactions occurring in the solution. The chemistry behind the actual etching process is more broadly described in literature [44–48]. One of the key points of the glass dissolution chemistry is that the HF solution is dissociated into various species; among which HF and HF_2^- mainly control the surface etching [44,49]. Both reactions are characterized by a negative reaction enthalpy. Thus, the etching reaction is a slightly exothermic reaction. For the purpose of wet etching, a Buffered HF solution with a stabilized HF activity (Buffer HF Improved or Buffer Oxide Etchant) is often used due to the toxicity of HF. In most etchant solutions, ammonium fluoride (NH_4F) acts as a buffering agent and controls the pH of the solution maintaining the HF concentration described by the following reaction [50]:



Etching is highly dependent on the temperature and concentration of the etchant solution. A high temperature and/or concentration of the etchant leads to the rapid dissolution of the glass surface. Moreover, stirring or agitation of the etchant solution also enhances the reduction of the cross section by promoting diffusion of the reactant to the fiber surface and removal of by-products. The etching rate is approximately double with a 10 $^\circ\text{C}$ increase in temperature at a given concentration of the solution [51]. However, high temperature, concentration, and presence of agitation in the etchant solution increase the evaporation rate of the solution making it hazardous to work with.

The buffered solution used in experiments was a mixture of NH_4F (40%) and HF (49%), combined in a volumetric ratio of 6:1. The solution had an HF concentration of 3.25 M and a pH of ~ 4 [51]. The small concentration of HF solution caused the etching process to be slow as compared to the heating and pulling method, but it allowed the generation of a stepped fiber tip with the continuity of the fiber core in addition to the desired change in the cross section. Additionally, it was possible to fabricate multiple cantilevered fibers at the same time allowing batch fabrication. The buffered solution had a vapor pressure and boiling temperature similar to that of water enabling the use of an etchant solution in an open system with limited evaporation. Furthermore, the presence of a floating plastic tray, as will be seen later, reduces

the open surface by a considerable amount. Thus, the amount of etchant evaporated during the etching process was very small and did not have any impact on the process.

With chemical etching, a tapered region ($\sim 600 \mu\text{m}$ axially) is often formed at the transition zone of the fiber. This tapering process occurs due to the capillary (meniscus) effect causing a slight rise of the HF solution with respect to the surface of the liquid along the optical fiber dipped in it. The HF that rises along the sidewalls of the fiber reduces its diameter, causing the tapered section [52]. Thus, the capillary effect can be blocked by preventing the presence of the etchant solution in contact with areas above the liquid interface of the dipped fibers. To accomplish this, a thin membrane of Ecoflex silicone rubber (Ecoflex 00–20, Smooth-On) was attached to a small plastic tray that floated on the surface of the HF. Small holes were drilled in the tray and the flexible membrane. The plastic protective coating on the fibers was stripped, and the fibers were passed through these holes, protruding $\sim 2 \text{ mm}$ into the HF solution. The flexible membrane closed the hole around the sidewalls of the fiber during the etching process, which prevented the solution from rising along the walls, and thus preventing the tapered region.

Fig. 2 shows the schematic of the setup used for the etching process. The buffered HF solution was held in a plastic container carrying the floating plastic tray with the fibers. This setup was placed inside a container of water and was placed on top of a hot plate; which guaranteed the uniform temperature of the solution during the etching process. Fibers were then taken out of the solution individually at specific time intervals and examined under the microscope to characterize their diameters.

As stated earlier, the etching process is greatly affected by the temperature of the etchant solution. To account for this variation, etching was repeated at different temperatures (from 23 $^\circ\text{C}$ to 35 $^\circ\text{C}$) by heating the water and the etchant solution using a hotplate. The water temperature was measured at regular intervals with a thermometer. As stated earlier, the etching reaction is slightly exothermic, but due to the large amount of the etchant solution and water, the temperature change during the process was very small ($< 1^\circ\text{C}$).

It is also possible to etch an optical fiber using an etchant solution in a vaporous state [53]. The overall etching reaction was the same as the one described earlier, with the difference being that there was condensation of the etchant vapour on the fiber surface, followed by the etching reaction, and the evaporation of the by-product [54].

As described earlier, the buffered solution is characterized with a small vapor pressure. Thus, the vapors generated at room temperature will be available in small amount. A high concentration HF (48%) solution was used to create the vapor etchant and was heated up to 35 $^\circ\text{C}$. The elevated temperature and high concentration of the etchant caused rapid vaporization, and a high etch rate. An Ecoflex membrane was

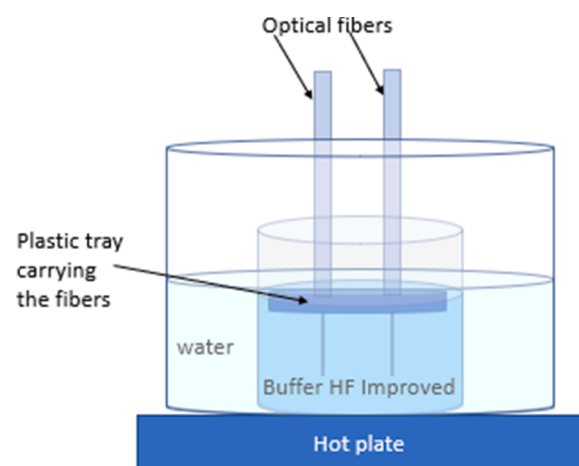


Fig. 2. The schematic of the setup used for etching the optical fibers.

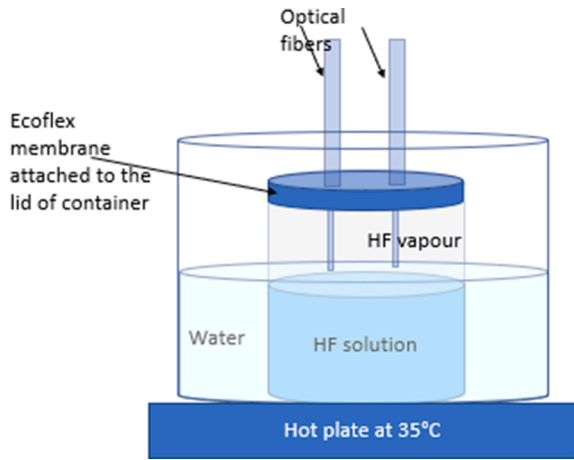


Fig. 3. The setup used for etching optical fibers at vaporous state.

attached to the bottom of the container’s lid, and fibers were inserted in the HF vapor via holes in the lid and membrane. The schematic diagram of the test setup is shown in Fig. 3.

3. Simulation of wet chemical etching

The etching process can be analytically modeled as a diffusion-controlled or a reaction-controlled process based on the reaction rate. Usually, the etching reaction is quite fast, and the process is controlled by the diffusion of the reactant species to the surface. The etchant flow impacts the process as well. Thus, convection needs to be considered in the calculations in case the etchant is not stationary. In our case, the etching process occurred in a stationary etchant solution, and no convection needed to be considered, which simplified the calculations.

The mathematical model describing the etching process can be either formulated using a moving grid approach [55,56] where the moving boundary tracks the etching process by change in shape, or a fixed grid approach [57,58]. In the latter case, the total concentration of the etchant solution given by the sum of reacted and unreacted portion is considered to be constant. The reacted concentration changes as the etching proceeds and allows for calculation of the etch front surface [59].

The governing equation describing the etching process is the mass diffusion equation described below:

$$\frac{\partial c}{\partial t} = D\nabla^2 c \tag{4}$$

where c is the concentration of HF solution, and D is the diffusion coefficient [53].

The velocity of the moving interface is given by:

$$v = -\frac{RM_{sub}}{m\rho_{sub}} \tag{5}$$

with R being the reaction rate at interface, M_{sub} , and ρ_{sub} being the molecular weight and the density of the optical fiber, respectively, and m is the stoichiometric reaction parameter from Eqs. (1) or (2) [53].

The etching process at the interface of fiber-etchant solution was simulated in COMSOL Multiphysics ambient using a moving boundary approach. It was possible to model the etching process as a 2D case due to the axial symmetry of the geometry. A zoomed version of the model geometry showing the optical fiber in an etchant solution schematized in Fig. 2. is shown in Fig. 4. The etchant solution surface in contact with the plastic tray was modelled as a surface with zero normal displacement. The white portion in Fig. 4. represents the section of the fiber under the etching process and the etched surface was considered as the deforming boundary. It was considered that the concentration of the etchant

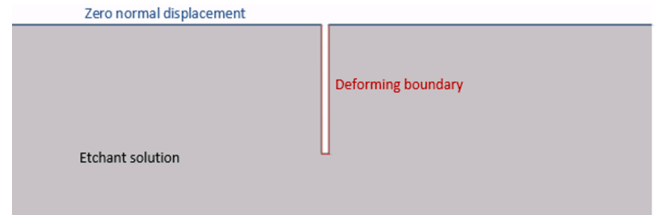


Fig. 4. 2D geometry of wet etching assembly with the prescribed boundary conditions.

solution was constant and equal to its initial value at the bottom surface of the etchant solution.

The diffusion of the etchant solution around the fiber interface was modelled using Transport of Diluted Species (chds) physics. In addition, the deformed geometry module described the moving geometry at the interface with velocity v . The diffusion coefficient for HF and HF_2 is $3 \times 10^{-9} \text{ m}^2/\text{s}$ [60].

4. Collection of reflected light

The flatness of the stepped interface surface at the transition section affects the collection efficiency of the reflected light. This can be characterized by sending light through the core of the fiber and capturing the reflected light from a target surface in front of the fiber. In the case of an irregular surface at the etched region, some of the incoming light will be further reflected or scattered away.

The schematic diagram of a setup to quantify these intensities is shown in Fig. 5, where P_0 , P_1 , and P_2 represent the laser power incident on the mirror, power backscattered from the transitional interface, and overall reflected light measured from the detector, respectively. There was no noise signal generated by the presence of ambient light. P_0 was measured by placing the detector in the mirror position. The back-scattered light from the transition zone was the power detected by an optical power meter, as in the setup of Fig. 5, by blocking the light beam between the objective lens and mirror. Thus, the power reflected by the mirror, P_3 , can be calculated as:

$$\text{Power reflected by mirror (P3)} = P_2 - P_1$$

A laser compatible with the used DCF ($\lambda = 1310 \text{ nm}$) was connected to the proximal end of the fiber with the help of a DCFC (DC1300LEFA, Thorlabs). The DCFC was designed to have the inner cladding of the DCF fused with a $200 \mu\text{m}$ core of a parallel MMF to siphon off power in the inner cladding towards the detector. The schematic diagram of the internal structure of a DCFC is shown in Fig. 6 (taken with the permission of [61]). The light in the single mode core was transmitted with no loss, while the multimode transfer had a ratio of output (port B) to input (port S) signal of $\geq 60\%$ [61].

The optical diagram, illustrated in Fig. 6, depicts the illumination and detection path of the light. The objective lens was placed at the focal length ($\sim 16.5 \text{ mm}$) away from the fiber tip and collimated the incoming

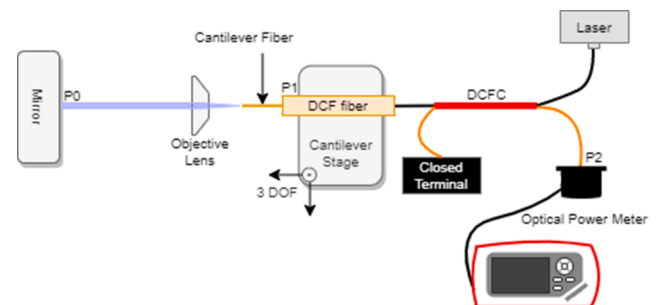


Fig. 5. The schematic diagram for the capture of reflected light from a mirror.

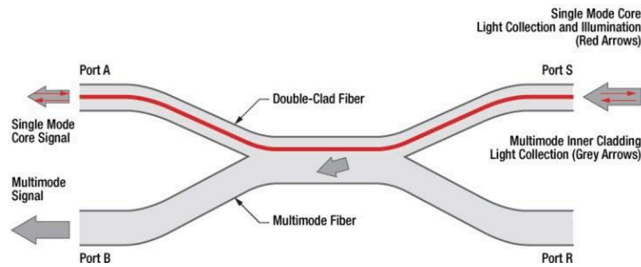


Fig. 6. Schematic diagram of an DCFC (taken with the permission of [61]).

light to the mirror surface, which transmitted the reflected light towards the fiber cladding.

Thus, the efficiency of the DCF system is defined as:

$$\eta = \frac{P2 - P1}{P0} \tag{6}$$

Due to the flat or irregular surface, some of the light was back reflected at the interface region. Back reflection, or optical return, is an undesirable effect in the fibers and is characterized by the contrast between the amount of light reflected by the mirror (P3) and the back-reflected light measured by blocking the light towards the mirror (P1):

$$Contrast = \frac{P3}{P1} \tag{7}$$

5. Results and discussion

The heating and pulling technique described above requires the interconnection between the cross sections of two different fibers by melting their ends at the glass transition temperature and connecting them together. The microscopic images of the fibers during different steps of the process are shown in Fig. 7. From the figure, it can be seen that in the first step, the cross section is reduced to the desired dimensions, then aligned with the fiber having the original cross section and spliced together. From Fig. 7, it can be seen that the process generated a quasi-flat surface at the transition region between the large and small sections of the fiber.

One of the drawbacks of this method was that a fraction of the excitation light from the laser device was scattered and lost at the spliced region. Thus, a higher light intensity was required to illuminate the target, and the leaked light added to the background noise in the target sample. It is reported in the literature that the reheating of the silica fibers leads to the reduction of strength of the fibers by the adhesion of solid particles to the fiber’s surface causing residual stresses in the

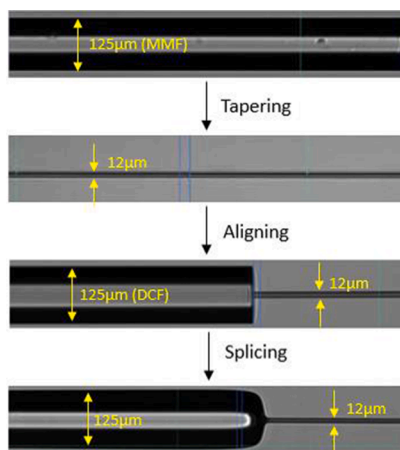


Fig. 7. Microscopic images of fabrication process of cantilevered fiber using heating and pulling method.

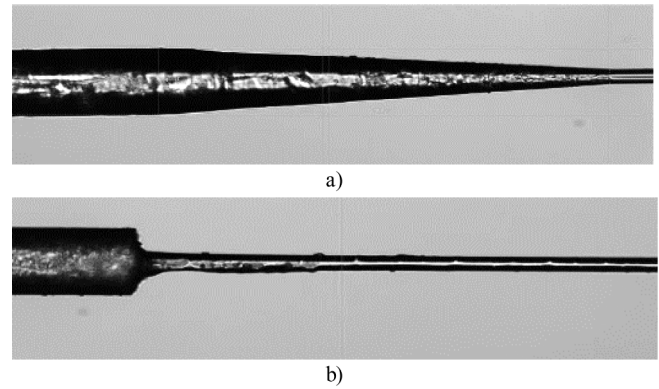


Fig. 8. The cross section of the fiber after etching in: a) an open surface; b) presence of an Ecoflex membrane.

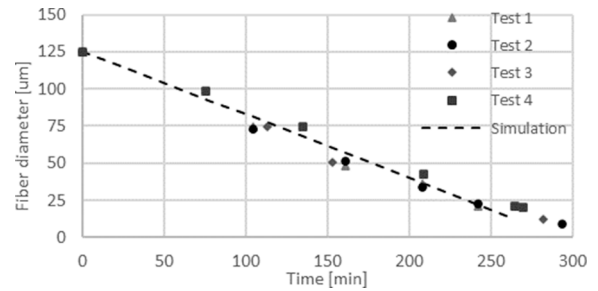


Fig. 9. Fiber diameter in time during etching at 23 °C.

spliced area [62,63]. In the Vytran splicing setup used in here, a high-purity Argon gas flowed over the fibers during fusion step to enable a clean spliced region without degrading the mechanical strength of the joint [64].

In the chemical etching process, the fiber was dipped into a buffer etchant solution. In an open container, etchant solution rose along the fiber at the open interface surface due to capillary action and caused the tapering of the cross section as can be seen in Fig. 8a. The tapered region created by the etching solution at ambient temperature is ~ 600 µm. The flat interface was generated through the use of an Ecoflex membrane to prevent the rise of solution up the sides of the fiber. It provided a quasi-flat interface surface as can be seen in Fig. 8b where the tapered region is less than 90 µm.

The wet etching process was evaluated at different temperatures within the 23 °C-35 °C range. The simulation results at 23 °C are compared with the experimental results in Fig. 9. The etching process was repeated multiple times to evaluate the reproducibility of the process and check the variance of results. Some of test results performed at the same conditions are shown in Fig. 9 as test 1 to test 4 and compared with theoretical simulation results showing the compatibility between the results.

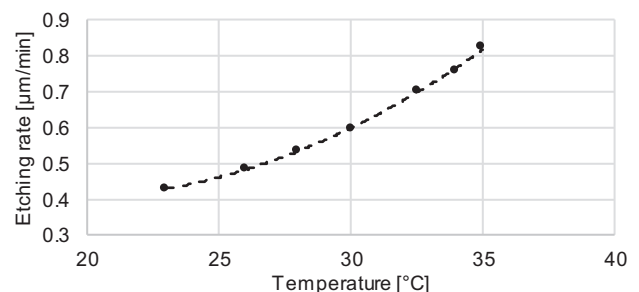


Fig. 10. Etching rate in function of water temperature.

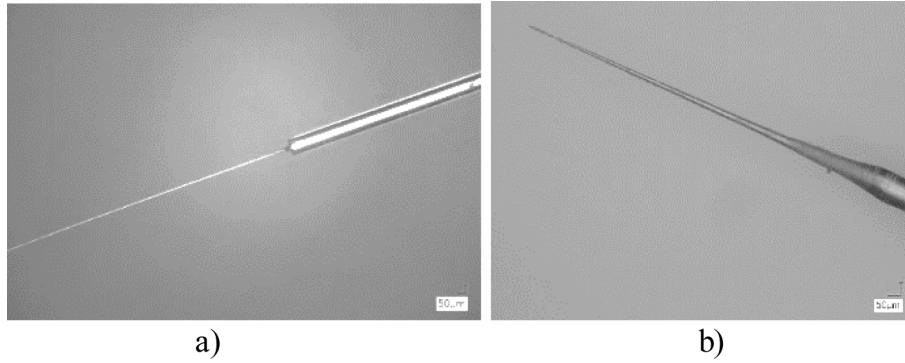


Fig. 11. Etched fibers: (a) using liquid HF solution; (b) using HF vapor.

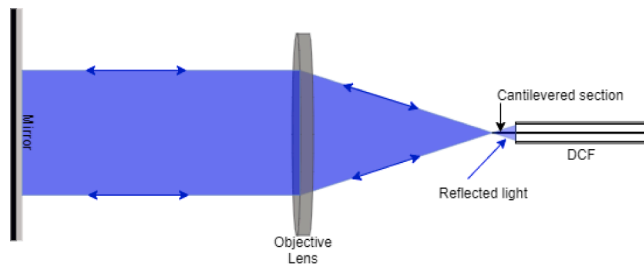


Fig. 12. Optical diagram of the proposed light collection setup.

The etching of optical fibers was repeated at different temperatures within the prescribed range, and an etching curve like Fig. 9 was obtained in each case. The trend of each curve defining the fiber diameter in time represents its etching rate and is recorded as a point in Fig. 10, which described the etching rate in function of temperature. As the temperature of the etchant solution increased, the etching rate continued to increase with a parabolic trend as can be seen in Fig. 10. The etched fiber obtained with this method as shown in Fig. 11a, had a quasi-smooth and linear surface.

In the case of fiber etching using HF in a vapor state, the concentration of the vapor decreased as the distance from the liquid surface increased. Thus, the fiber was etched more towards the free end, and the fiber was semi-linearly tapered as shown in Fig. 11b. Thus, etching using a vaporous state did not yield the desired stepped structure and was not further investigated.

The amount of light intensity collected by the cladding of cantilevered fiber samples is considered following the schematic of Fig. 12. In the case of a cleaved DCF with no cantilevered portion, the light incoming from the core of the DCF was 12.35mW, while the measured reflected light was 7.41mW, and the optical return was 72.1 μW. Thus, the efficiency (η) was $\sim 59.33\%$, while the contrast was 101.78.

In the case of the spliced fiber, the light incoming from the laser was 3.425mW, but there was some power leakage at the spliced region due to imperfect alignment of the cores. The light intensity at the fiber tip was much smaller and varied among the samples depending on the light transmission at the transient section. The parameters characterizing the collection of reflected light for three different cantilevered fibers are reported in Table 1.

Table 1
Light transmission properties through the fibers fabricated using the heating and pulling method.

Sample number	Transmission in spliced section	Light intensity at fiber tip (P0)	Measured reflected light (P2)	Optical return (P1)	η	Contrast
1	86.26%	2.96mW	0.154mW	0.007mW	4.95%	20.68
2	64.82%	2.22mW	0.213mW	0.031mW	8.21%	5.96
3	89.17%	3.05mW	0.148mW	0.007mW	4.64%	21.49

Similar data obtained for the chemically etched fibers is summarized in Table 2. In this case, no light leakage occurred in the transition zone due to etching of just the cladding surface. Thus, the light intensity at the fiber tip was much higher compared to the heating and pulling method.

From the measured data, it can be summarized that the efficiency and the contrast of the samples were highly variable among the samples fabricated using both methods. In the case of the heating and pulling method, it was mainly a function of the filament power, the alignment of the DCF fiber, and the taper of the MMF fiber.

In chemically etched fibers, the flatness at the interface surface is highly dependent on the straightness of the fiber in the plastic tray. The variability among the samples was avoided by placing the fibers perpendicular to the etchant surface, which will also result in a nice flat stepped interface.

6. Conclusion

The fabrication processes to make micrometer sized double clad fiber tips with a step reduction of the cross section using the heating-pulling and the chemical etching methods are shown in this paper. Such fibers can be used as a resonant scanner by fixing the larger section and exciting the thin section of the fiber with a micro-actuator. In the first fabrication process, an MMF was tapered down and spliced to a DCF. In the second technique, a buffered etchant solution with stabilized HF activity was used to etch the fibers. To get a flat transition, a flexible membrane was attached on the bottom surface of a plastic tray holding the fibers. The flexibility of the membrane caused the continuous closure of the membrane around the fiber and prevented the formation of a meniscus that caused tapering in the fiber. Wet etching was performed using the etchant solution at vaporous and liquid states, with the latter

Table 2
Light transmission properties through the fibers fabricated using the etching method.

Sample number	Light Intensity at fiber tip (P0)	Measured reflected light (P2)	Optical return (P1)	η	Contrast
1	11.58mW	1.252mW	0.243mW	8.71%	4.15
2	11.58mW	0.463mW	0.034mW	3.70%	12.67
3	11.58mW	1.882mW	0.041mW	15.89%	44.45

one allowing the fabrication of smooth surfaced stepped fibers.

Some of the advantages of using chemical etching over the heating and pulling method are:

- Continuity of the core at the transition zone. Thus, the light coming from the laser is nearly 100% transmitted to the distal end of the fiber.
- No light leakage at the interface section causing less power needed to illuminate the target sample.
- Possibility of batch fabrication of the fiber samples, i.e. many fibers can be produced at the same time.
- The cantilever portion can be made as large as desired by dipping a large portion of the fiber inside the etching solution. However, in the heating and pulling method, the thin sections are limited to a length of a few millimeters due to mechanical resistance.
- Very thin section fibers can be fabricated as compared to the heating and pulling method.
- Consistency of geometry among the different samples.

Notwithstanding, HF is a volatile chemical to work with; although this drawback can be eliminated by using a less concentrated or buffered etching solution.

Moreover, in the case of the heating and pulling method, the properties of the fibers depended on the age of the heating element causing variability among the samples. In addition, depending on the fusion conditions, heating of an optical fiber can degrade its mechanical strength, while the etching using HF does not affect its strength.

To conclude, wet etching is preferred over the heating and pulling method to fabricate the micrometer sized stepped fiber tips with a flat interface surface, which can find use in sub-micrometer sized optical scanners and sensors.

CRedit authorship contribution statement

Mandeep Kaur: Conceptualization, Data curation, Validation, Formal analysis, Investigation, Writing - original draft. **Geoffrey Hohert:** Software, Methodology, Writing - review & editing. **Pierre M. Lane:** Software, Writing - review & editing, Supervision. **Carlo Menon:** Supervision, Project administration, Funding acquisition.

Declaration of Competing Interest

The authors declare that they have no known competing financial interests or personal relationships that could have appeared to influence the work reported in this paper.

Acknowledgements

The authors would like to acknowledge Canada Research Chair (CRC) program, and Mitacs internship program for their financial support.

References

- [1] J.P. Powers, *An introduction to fiber optic systems*, Irwin, Chicago, 1997.
- [2] N. Alberto, C. Tavares, M.F. Domingues, S.F.H. Correia, C. Marques, P. Antunes, J. L. Pinto, R.A.S. Ferreira, P.S. André, Relative humidity sensing using micro-cavities produced by the catastrophic fuse effect, *Opt. Quant. Electron.* 48 (3) (2016), <https://doi.org/10.1007/s11082-016-0491-4>.
- [3] Optromix, "FBG Sensors," optromix, [Online]. Available: <https://fibergratings.com/products/fbg-sensors/>. [Accessed 10 November 2020].
- [4] K. Yuksel, D. Kinet, K. Chah, C. Caucheteur, *Sensors* 20 (6) (2020) 1–10.
- [5] A.G. Mignani, F. Baldini, Fiber-optic sensors in health care, *Phys. Med. Biol.* 42 (5) (1997) 967–979.
- [6] A.G. Mignani, F. Baldini, Biomedical sensors using optical fibers, *Rep. Prog. Phys.* 59 (1) (1996) 1–28.
- [7] Luxtron, "Fiber Optic Temperature Sensors," Advanced Energy, 2020. [Online]. Available: <https://www.advancedenergy.com/products/temperature-measurement/fiber-optic-temperature-sensors/>. [Accessed 10 November 2020].
- [8] Amphenol, "NovaSensor | Pressure Sensors," NovaSensor, May 2019. [Online]. Available: <https://amphenol-sensors.com/en/novasensor>. [Accessed 10 November 2020].
- [9] Perimed, "PeriFlux," Perimed, 2020. [Online]. Available: <https://www.perimed-instruments.com/content/assessment-and-diagnostics/>. [Accessed 12 November 2020].
- [10] F. Baldini, "Bile Sensor: from the lab to the market," in *Proc. SPIE 3860*, Boston (USA), 1999.
- [11] R. Correia, S. James, S.-W. Lee, S.P. Morgan, S. Korposh, Biomedical application of optical fibre sensors, *J. Opt.* 20 (7) (2018) 1–25, 073003.
- [12] A. Leal-Junior, L. Avellar, A. Frizzera, C. Marques, Smart textiles for multimodal wearable sensing using high stretchable multiplexed optical fiber system, *Sci. Rep.* 10 (1) (2020) 13867.
- [13] A. Leal-Junior, A. Frizzera, C. Marques, M.J. Pontes, Polymer-optical-fiber-based sensor system for simultaneous measurement of angle and temperature, *Appl. Opt.* 57 (7) (2018) 1717–1723.
- [14] A. Issatayeva, A. Beisenova, D. Tosi, C. Molardi, Fiber-Optic Based Smart Textiles For Real-Time Monitoring Of Breathing Rate, *Sensors* 20 (12) (2020) 1–16, 3408.
- [15] Z. Gong, Z. Xiang, X.O. Yang, J. Zhang, N. Lau, J. Zhou, C.C. Chan, Wearable fiber optic technology based on smart textile: a review, *Materials* 12 (20) (2020) 1–15, 3311.
- [16] F. Helmchen, Miniaturization of Fluorescence Microscopes Using Fibre Optics, *Exp. Physiol.* 87 (6) (2002) 737–745.
- [17] C.J. Engelbrecht, R.S. Johnston, E.J. Seibel, F. Helmchen, Ultra-compact fiber-optic two-photon microscope for functional fluorescence imaging in vivo, *Opt. Express* 16 (8) (2008) 5556–5564.
- [18] X. Liu, M.J. Cobb, Y. Chen, M.B. Kimmey, X. Li, Rapid-scanning forward-imaging miniature endoscope for real-time optical coherence tomography, *Opt. Lett.* 29 (15) (2004) 1763–1765.
- [19] C.-P. Liang, J. Wierwille, T. Moreira, G.S. Schwartzbauer, M.S. Jafri, C.-M. Tang, Y. Chen, A forward-imaging needle-type OCT probe for image guided stereotactic procedures, *Opt. Express* 19 (27) (2011) 26283–26294.
- [20] L. Wu, Z. Ding, G. Huang, Realization of 2D scanning pattern of a fiber cantilever by nonlinear coupling. *Fifth International Conference on Photonics and Imaging in Biology and Medicine*, 2006.
- [21] B. Sun, H. Nogami, Y. Pen, R. Sawada, Microelectromagnetic actuator based on a 3D printing process for fiber scanner application, *J. Micromech. Microeng.* 25 (7) (2015) 1–8, 075014.
- [22] Y.-H. Seo, K. Hwang, H.-C. Park, K.-H. Jeong, Electrothermal mems fiber scanner with lissajous patterns for endomicroscopic applications, *Opt. Express* 24 (4) (2016) 3903–3909.
- [23] J. Yao, T. Peng, B. Sun, H. Zhang, M. Zhao, B. Dai, H. Liu, G. Ding, R. Swada, Z. Yang, A Single-Fiber Endoscope Scanner Probe Utilizing Two-Degrees-of-Freedom (2DOF) High-Order Resonance to Realize Larger Scanning Angle, *IEEE Trans. Compon. Packag. Manuf. Technol.* 9 (12) (2019) 2332–2340.
- [24] H.-C. Park, X. Zhang, W. Yuan, L. Zhou, H. Xie, X. Li, Ultralow-voltage electrothermal MEMS based fiber-optic scanning probe for forward-viewing endoscopic OCT, *Opt. Lett.* 44 (9) (2019) 2232–2235.
- [25] H.-C. Park, Y.-H. Seo, K.-H. Jeong, Lissajous fiber scanning for forward viewing optical endomicroscopy using asymmetric modulation, *Opt. Express* 22 (5) (2014) 5818–5825.
- [26] M. Kaur, P.M. Lane, C. Menon, Endoscopic Optical Imaging Technologies and Devices for Medical Purposes: State of the Art, *Applied Sciences* 10 (19) (2020) 1–34, 6865.
- [27] M.T. Myaing, D.J. MacDonald, X. Li, Fiber-optic scanning two-photon fluorescence endoscope, *Opt. Lett.* 31 (8) (2006) 1076–1078.
- [28] A.A. Ahrabi, M. Kaur, Y. Li, P. Lane, C. Menon, An Electro-Thermal Actuation Method for Resonance vibration of a Miniaturized Optical-Fiber Scanner for Future Scanning Fiber Endoscope Design, *Actuators* 8 (21) (2019) 1–18.
- [29] M. Kaur, M. Brown, P.M. Lane, C. Menon, An Electro-Thermally Actuated Micro-Cantilever-Based Fiber Optic Scanner, *IEEE Sens. J.* 20 (17) (2020) 9877–9885.
- [30] P.K. Sarkar, A. Halder, A. Adhikari, N. Polley, S. Darbar, P. Lemmens, S.K. Pal, DNA-based fiber sensor for direct in-vivo measurement of oxidative stress, *Sens. Actuators, B* 255 (2018) 2194–2202.
- [31] M. Tao, Y. Jin, N. Gu, L. Huang, A method to control the fabrication of etched optical fiber probes with nanometric tips, *J. Opt.* 015503 (2010).
- [32] N. Van Toan, M. Toda and T. Ono, "An Investigation of Process for Glass Micromachining," *Micromachines*, vol. 7, no. 51, 2016.
- [33] P. Lambelet, A. Sayah, M. Pfeffer, C. Philipona, F. Marquis-Weible, Chemically etched fiber tips for near-field optical microscopy: a process for smoother tips, *Appl. Opt.* 37 (1998) 7289–7292.
- [34] H.J. Khashi, Fabrication of Submicron-Diameter and Taper Fibers Using Chemical Etching, *J. Mater. Sci. Technol.* 28 (4) (2012) 308–312, [https://doi.org/10.1016/S1005-0302\(12\)60059-0](https://doi.org/10.1016/S1005-0302(12)60059-0).
- [35] B. Puygranier, P. Dawson, Chemical etching of optical fibre tips - experimental and model, *Ultramicroscopy* 85 (2000) 235–248.
- [36] J.M. Ward, D.G. O'Shea, B.J. Shortt, M.J. Morrissey, K. Deasy, S.Íle.G. Nic Chormaic, Heat-and-pull rig for fiber taper fabrication, *Rev. Sci. Instrum.* 77 (8) (2006) 083105, <https://doi.org/10.1063/1.2239033>.
- [37] C.H. Chao, S.C. Shen, J.R. Wu, Fabrication of 3-D Submicron Glass Structures by FIB, *J. of Mater. Eng and Perform* 18 (7) (2009) 878–885, <https://doi.org/10.1007/s11665-008-9318-1>.
- [38] T. Ichiki, Y. Sugiyama, T. Ujiie, Y. Horiike, Deep dry etching of borosilicate glass using fluorine based high-density plasmas for microelectromechanical system fabrication, *J. Vac. Sci. Technol., B* 21 (5) (2003) 2188–2192.

- [39] H.M. Presby, A.F. Benner, C.A. Edwards, Laser micromachining of efficient fiber microlenses, *Appl. Opt.* 29 (18) (1990) 2692–2695.
- [40] L. Xu, L. Jiang, S. Wang, B. Li, Y. Lu, High-temperature sensor based on an abrupt-taper Michelson interferometer in single-mode fiber, *Optical Society of America* 52 (10) (2013) 2038–2041.
- [41] M. Shao, Y. Zang, X. Qiao, H. Fu, Z.-A. Jia, Humidity Sensor Based on Hybrid Fiber Bragg Grating/Abrupt Fiber Taper, *IEEE Sens. J.* 17 (5) (2017) 1302–1305.
- [42] N.-K. Chen, Z.-Y. Chen, K.-Y. Lou, W.-H. Cheng and C. Lin, “Elongated abruptly tapered micro fiber interferometer for nanoparticles attraction and analyses,” in 2015 Conference on Lasers and Electro-Optics, San Jose, CA, 2015.
- [43] R.M. Chyad, M.Z.M. Jafri, K.U. Ibrahim, Fabrication nano fiber optic by chemical etching for sensing application, *Eng. & Tech. J.* 33 (6) (2015) 994–1002.
- [44] J.S. Judge, A Study of the Dissolution of SiO₂ in Acidic Fluoride Solutions, *J. Electrochem. Soc.* 118 (11) (1971) 1172–1175.
- [45] H. Proksche, G. Nagorsen, The Influence of NH₄F on the Etch Rates of Undoped SiO₂ in Buffered Oxide Etch, *J. Electrochem. Soc.* 139 (2) (1992) 521–524.
- [46] S. Verhaverbeke, I. Teerlinck, C. Vinckier, G. Stevens, R. Cartuyvels, M.M. Heyns, The Etching Mechanisms of SiO₂ in Hydrofluoric Acid, *The Journal of the Electrochemical Society* 141 (10) (1994) 2852–2857.
- [47] K. Osseo-Asare, Etching Kinetics of Silicon Dioxide in Aqueous Fluoride Solutions: A Surface Complexation Model, *J. Electrochem. Soc.* 143 (4) (1996) 1339–1347.
- [48] B. Shvartsev, D. Gelman, I. Komissarov, A. Epshtein, D. Starosvetsky, Y. Ein-Eli, Influence of Solution Volume on the Dissolution Rate of Silicon Dioxide in Hydrofluoric Acid, *ChemPhysChem* 16 (2) (2015) 370–376, <https://doi.org/10.1002/cphc.201402627>.
- [49] H. Kikuyama, M. Waki, I. Kawanabe, M. Miyashita, T. Yabune, N. Miki, J. Takano, T. Ohmi, Etching Rate and Mechanism of Doped Oxide in Buffered Hydrogen Fluoride Solution, *J. Electrochem. Soc.* 139 (8) (1992) 2239–2243.
- [50] V. Talla, “BOE Wet Etch of Silicon Dioxide,” 08 05 2011. [Online]. Available: <http://labs.ece.uw.edu/cam/SOPs/BOE%20Wet%20Etching%20of%20SiO2%20SOP.pdf>. [Accessed 14 08 2020].
- [51] “Silicon Dioxide (SiO₂) Etchants,” Transene Company, Inc., [Online]. Available: <https://transene.com/sio2/>. [Accessed 14 08 2020].
- [52] A. Foti, C. D’Andrea, F. Bonaccorso, M. Lanza, E. Messina, E. Messina, O. M. Marago, B. Fazio, P.G. Gucciardi, A Shape-Engineered Surface-Enhanced Raman Scattering Optical Fiber Sensor Working from the Visible to the Near-Infrared, *Plasmonics* 8 (2013) 13–23.
- [53] J. Bierlich, J. Kobelke, D. Brand, K. Kirsch, J. Dellith, H. Bartelt, Nanoscopic Tip Sensors Fabricated by Gas Phase Etching of Optical Glass Fibers, *Photonic Sensors* 2 (4) (2012) 331–339.
- [54] C.R. Helms, B.E. Deal, Mechanisms of the HF/H₂O vapor phase etching of SiO₂, *Journal of Vacuum Science & Technology A* 10 (4) (1992) 806–811.
- [55] H.K. Kuiken, “Etching: A Two-Dimensional Mathematical Approach,” *Proceedings of the Royal Society of London. Series A, Mathematical and physical sciences*, vol. 392, no. 1802, pp. 199–225, 1984.
- [56] C.B. Shin, D.J. Economou, Effect of Transport and Reaction on the Shape Evolution of Cavities during Wet Chemical Etching, *J. Electrochem. Soc.* 136 (7) (1989) 1997–2004.
- [57] Y.C. Lam, J.C. Chai, P. Rath, H. Zheng, V.M. Murukeshan, A Fixed-Grid Method for Chemical Etching, *International Communications in Heat and Mass Transfer* 31 (8) (2004) 1123–1131.
- [58] P. Rath, J.C. Chai, H. Zheng, Y.C. Lam, V.M. Murukeshan, Modeling two-dimensional diffusion-controlled wet chemical etching using a total concentration approach, *Int. J. Heat Mass Transf.* 49 (7) (2006) 1480–1488.
- [59] P. Rath, J.C. Chai, Modeling convection-driven diffusion-controlled wet chemical etching using a total-concentration fixed-grid method, *Numerical Heat Transfer, Part B: Fundamentals* 53 (2) (2007) 143–159.
- [60] A. Ivanov, “Simulation of Electrochemical Etching of Silicon with COMSOL,” in *Proceedings of the 2011 COMSOL Conference*, Stuttgart, Germany, 2011.
- [61] Thorlabs, “2x2 Double-Clad Fiber Couplers,” Thorlabs, [Online]. Available: https://www.thorlabs.com/newgrouppage9.cfm?objectgroup_id=8400. [Accessed 16 November 2020].
- [62] J.T. Krause, C.R. Kurkjian, U.C. Paek, Strength of fusion splices for fibre lightguides, *Electron. Lett.* 17 (6) (1987) 232–233.
- [63] C.R. Kurkjian, M.J. Matthewson, J.M. Rooney, “Effects of heat treatment and HF etching on the strength of silica lightguides,” in *Reliability of Optical Fiber Components, Devices, Systems, and Networks II*, Bellingham, 2004.
- [64] “Vytran Filament Fusion Splicer,” Thorlabs, [Online]. Available: https://www.thorlabs.com/newgrouppage9.cfm?objectgroup_id=9355. [Accessed 16 November 2020].